Icarus 206 (2010) 74–82

Contents lists available at ScienceDirect

Icarus

journal homepage: www.elsevier.com/locate/icarus

A plasma flow velocity boundary at Mars from the disappearance of electron plasma oscillations

F. Duru [a,*], D.A. Gurnett [a], J.D. Winningham [b], R. Frahm [b], R. Modolo [a]

[a] Dept. of Physics and Astronomy, University of Iowa, Iowa City, IA 52240, USA
[b] Southwest Research Inst., PO Drawer 28510, San Antonio, TX 28510, USA

ARTICLE INFO

Article history:
Received 5 September 2008
Revised 3 April 2009
Accepted 4 April 2009
Available online 9 May 2009

Keywords:
Ionospheres
Mars
Solar wind

ABSTRACT

The Mars Advanced Radar for Subsurface and Ionospheric Sounding (MARSIS) on the Mars Express (MEX) spacecraft is capable of measuring ionospheric electron density by the use of two main methods: remote radar sounding and from the excitation of local plasma oscillations. The frequency of the locally excited electron plasma oscillations is used to measure the local electron density. However, plasma oscillations are not observed when the plasma flow velocity is higher than about 160 km/s, which occurs mainly in the solar wind and magnetosheath. As a consequence, in many passes, there is a sudden disappearance of the plasma oscillations as the spacecraft enters into the magnetosheath. This fact allows us to identify a flow velocity boundary on the dayside, between the ionosphere of Mars and the shocked solar wind. This paper summarizes the results of the measurement of 552 orbits mostly over a period from August 4, 2005 to August 17, 2007. The boundary points found using MARSIS have been verified by measurements from the Analyzer of Space Plasma and Energetic Atoms (ASPERA-3) Electron Spectrometer (ELS) instrument on Mars Express. The average position of the flow velocity boundary is compared to flow velocity simulations computed using hybrid model and other boundaries. The boundary altitude is slightly lower than the magnetic pile-up boundary determined using Phobos 2 and Mars Global Surveyor (MGS) crossings, but it is in good agreement with the induced magnetospheric boundary determined by ASPERA-3. Investigation of the effect of the crustal magnetic field revealed that the flow velocity boundary is raised at the locations with strong crustal magnetic fields.

1. Introduction

The Mars Advanced Radar for Subsurface and Ionospheric Sounding (MARSIS) is a low-frequency radar carried by the Mars Express (MEX) spacecraft, which entered an elliptical orbit around Mars on December 25, 2003 (Chicarro et al., 2004). MARSIS consists of a 40 m tip-to-tip dipole antenna, a 7 m monopole antenna, a radio transmitter, a receiver, and a digital signal processing system. The MARSIS is designed to perform subsurface and ionospheric radar soundings (Picardi et al., 2004). The ionospheric sounding results of MARSIS were reported by several papers including Gurnett et al. (2005, 2008). A typical ionospheric sounding pass, which starts at an outbound altitude of about 1300 km, goes down to an inbound altitude of about 250 km, and then ends at an outbound altitude of about 1300 km, lasts for about 36 min and provides about 285 frequency scans. The basic sweep cycle is repeated once every 7.54 s.

With MARSIS, it is possible to obtain ionospheric electron densities in two different ways. The first method is via remote radar sounding of the ionosphere, where a short radio pulse of fixed frequency f is sent, and the time delay of the returning echo due to vertical reflection from the horizontally stratified ionosphere is measured (Gurnett et al., 2005). With this method, electron density values at altitudes between about 130 and 400 km are obtained. The second method is based on the excitation of local electron plasma oscillations. In the ionospheric sounding mode, the sounder transmitter excites electrostatic electron plasma oscillations at the local electron plasma frequency. Since the electron plasma oscillations are usually very intense, they cause clipping in the receiver, which due to distortion introduces harmonics of the basic oscillation frequency (see Duru et al., 2008). Due to the chirping of the amplifier, these harmonics are seen as equally spaced vertical lines on the color-coded plots of echo intensity as a function of time delay and frequency (ionograms) (Gurnett et al., 2005; Duru et al., 2008). In many cases, the fundamental of the electron plasma frequency cannot be observed, since it is below the low frequency cutoff of the receiver (100 kHz). However, by measuring the spacing between the harmonics, electron plasma frequencies can still be measured. With this method it is often possible to measure

* Corresponding author. Address: Dept. of Physics and Astronomy, The University of Iowa, 203 Van Allen Hall, Iowa City, IA 52242-1479, USA.
E-mail address: firdevs-duru@uiowa.edu (F. Duru).

0019-1035/$ - see front matter © 2009 Elsevier Inc. All rights reserved.
doi:10.1016/j.icarus.2009.04.012

the local electron plasma frequency at very high altitudes, as high as 1300 km, where the electron densities are very low (Gurnett et al., 2005; Duru et al., 2008). A study of local electron densities using this technique has been published by Duru et al. (2008). Local electron plasma frequencies obtained by using the above method, are converted into electron densities by using $n_e = (f_p/8980)^2$, where n_e is the electron density in cm^{-3}, and f_p is electron plasma frequency in Hz (Gurnett and Bhattacharjee, 2005).

It is observed that, in many passes, the electron plasma oscillations disappear suddenly as the spacecraft altitude increases. As stated in Duru et al. (2008), electron plasma oscillations are not detectable when (a) the flow velocity of the plasma is higher than about 160 km/s, (b) the electron density is lower than 10 cm^{-3}, and (c) the plasma temperature is higher than about 80,000 K. It should be noted that all three of the above cases are satisfied in a solar wind like plasma which is hot, tenuous and fast. The flow velocity of the plasma plays an especially important role in the disappearance of the electron plasma oscillations on the dayside. With MARSIS, there is a minimum time delay between sending and receiving the signal, that can be resolved, which is about 0.25 ms. As stated in Duru et al. (2008), when calculating the plasma frequency thermal effects are ignored as in cold plasma theory and it is assumed that the oscillation frequency is at the electron plasma frequency ($\omega = \omega_{pe}$). Since the oscillation frequency does not depend on the wave number (k), group velocity ($v_g = \delta\omega/\delta k$) is zero and the waves are frozen within the plasma. In order to generate a response in the receiver, the wave packet must stay in the vicinity of the spacecraft for at least 0.25 ms. Since the size of the wave packet is comparable to the size of the dipole antenna (40 m), no response is expected when the spacecraft is in a plasma with flow velocities higher than (40 m/0.25 ms =) 160 km/s, because the oscillating wave packet excited by the transmitter is carried away from the antenna before the first measurement is made (Duru et al., 2008). This velocity determination makes sense independent of the antenna. The electric field is parallel to the k vector and the dominant electric field is along the antenna. The group velocity is zero in the plasma rest frame. It is independent of k vector. Velocities with the magnitude calculated above are observed in the solar wind or the magnetosheath, not in the ionosphere. Therefore, the sudden disappearance of the plasma oscillations at high altitudes can be explained by the transition of the spacecraft from the ionosphere of Mars to the shocked solar wind. A summary of both observations and simulations on the plasma environment of Mars is provided by Nagy et al. (2004).

In the ionograms (Fig. 1), the fundamental and the harmonics of the electron plasma frequency are visible in the color spectrogram

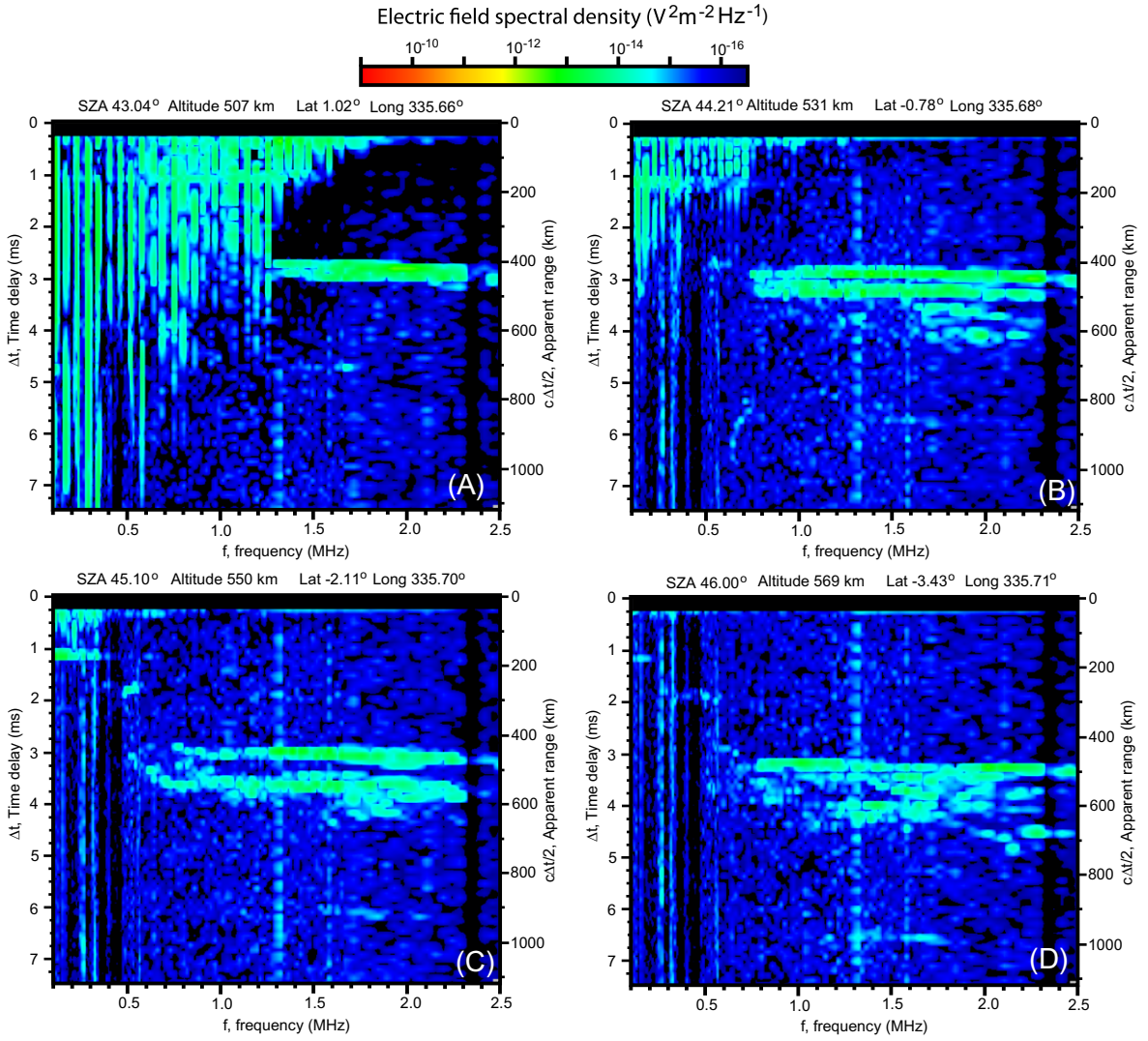

Fig. 1. Four ionograms, from day July 18, 2006, orbit no 3238, showing the decrease in the duration of the electron plasma oscillation harmonics, corresponding to an increase in the flow velocity, as the spacecraft approaches the boundary. The spacecraft gets closer to the boundary as we go from ionogram A to ionogram D. On the fourth ionogram, labeled with D, the spacecraft enters the shocked solar wind.

and are seen as equally spaced vertical lines. The time delay is shown on the *y*-axis. Therefore, the length of the vertical lines gives the duration of the fundamental and the harmonics of the electron plasma frequency. Most of the time, the duration of the electron plasma oscillation fundamental and harmonics decreases as the spacecraft approaches the boundary. This monotonic decrease in the duration length supports the idea that the electron density oscillations disappear due to increasing flow velocity of the plasma. Fig. 1 provides four ionograms from a pass on July 18, 2006. In each of these plots, time delay is along the vertical axis, the frequency is on the horizontal axis and the color code gives the echo strength. The spacecraft approaches the boundary as we go from ionogram A to ionogram D. In ionogram A, the first few electron plasma harmonics have durations higher than 7 ms, implying a low flow velocity at the position of the spacecraft. The increase in the flow velocity of the plasma results in a decrease in the amount of time the spacecraft can detect the wave packet. Therefore, the duration of the harmonics in the ionograms decreases as the spacecraft gets closer to the boundary. At the boundary (shown by the ionogram D), they disappear completely, due to high enough flow velocity, which carries the wave packet away before any measurement can be obtained. In every ionogram there are some extra vertical lines (such as the one seen at around 1.3 MHz), which are not part of the harmonics. As can be seen in the ionograms, these lines are always observed at the same frequencies and they look different than harmonic lines. They appear as dashed lines and are of instrumental origin. Fig. 2 provides numerical values for the electron density and plasma flow velocity changes obtained during the same pass as in Fig. 1, as the spacecraft goes towards the magnetosheath. The minimum velocity values are obtained by dividing the length of the antenna by the corresponding duration value (v_{min} = 40 m/Δt). The top panel shows the electron density as a function of time. The spacecraft approaches the boundary as the numbers on the *x*-axis increase, indicating the universal time in 7.54 s steps after 08:23:01.122 UT. The electron density decreases as the spacecraft approaches the boundary. The last electron density value, measured 7.54 s before the boundary is about 18 cm^{-3}, which is higher than the lowest measurable electron density value, 10 cm^{-3}, indicated by the black line. The letters A, B, and C show the ionograms (in Fig. 1) corresponding to the given points. A sketch of the trajectory for this pass is provided in the upper right corner of the figure. The bottom panel gives the duration of the third harmonic corresponding to the electron densities in the above panel. Usually, the first few harmonics are stronger and seen clearly in the ionograms. On the other hand, as explained above, when the frequency of the fundamental or the harmonics of the electron plasma oscillations is lower than the lower frequency limit of the receiver, they cannot be observed in the ionograms. In this figure, third harmonic is chosen to study the change in the duration since its frequency is above the lower limit of the receiver and provides a clear picture in each of the ionograms. In the bottom panel, for the first three points, time delay is more than 7 ms, meaning the flow velocity is low enough for the wave packet to remain in the vicinity of the spacecraft long enough to be seen in the ionogram. Starting from the 4th point, the duration begins to decrease. It decreases monotonically until the 8th point. The 9th point in this series cannot be shown on Fig. 2 since it is where the electron plasma oscillations can no longer be seen in the ionograms. At this point, the spacecraft is in a region where the plasma flow velocity exceeds about 160 km/s and the electron plasma oscillations are swept away from the vicinity of the spacecraft before they can be detected. In about 75% of the boundary crossings the duration of the plasma oscillation decreases systematically (corresponding to an increase in flow velocity). In about 6% of the cases, the decrease in the duration is so sudden that the plasma oscillations disappear completely in the 7.54 s between successive measurements. In the remainder of the cases, the duration of the plasma oscillations increases and decreases before disappearing completely from the ionograms.

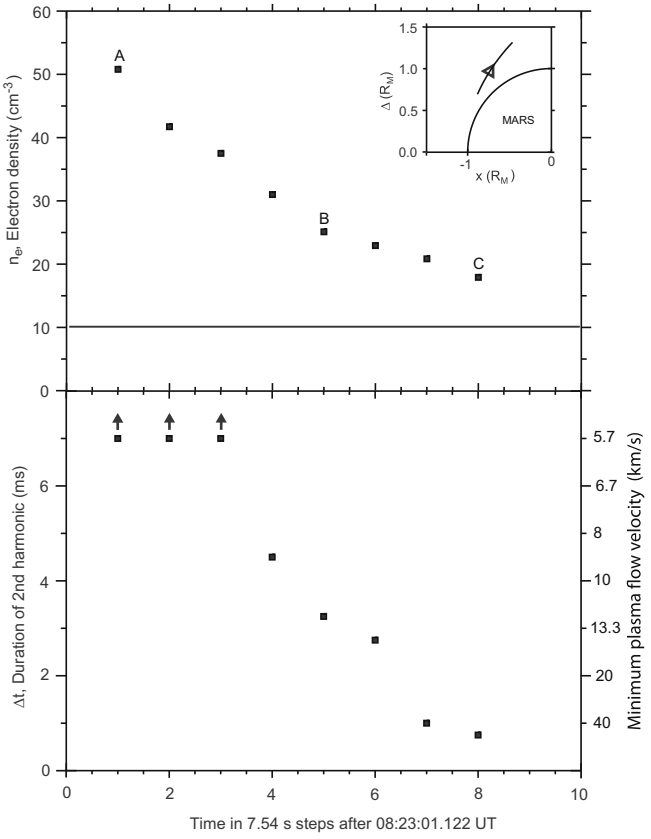

Fig. 2. The change in the electron density and flow velocity as the spacecraft approaches the boundary (same pass as in Fig. 1). The bottom panel shows the time delay of the third harmonic, which is inversely proportional to the plasma flow velocity. The corresponding minimum plasma flow velocities are given on the right side of the bottom panel. A sketch of the trajectory of the given pass is provided on the upper right corner of the figure.

Investigation of the electron density data right before the boundary showed that the electron density is usually significantly higher than the lowest value we can measure with our method. Only in 11 boundary crossings is the electron density just before the boundary equal to or lower than 15 cm^{-3}, which is much higher than the minimum electron density that MARSIS can detect using the electron oscillation technique. The lower electron density limit which can produce detectable harmonics is ~1 $cm^{-3}$and the minimum electron density that can be measured reliably with this technique is ~10 cm^{-3}. Also, the fact that the highest plasma temperatures in the ionosphere of Mars are predicted to be around 5000 K (Nagy et al., 2004), suggests that temperatures around 80,000 K, where Landau damping becomes important for an electron density value ~10 cm^{-3}, are unlikely at the locations where the boundary crossings occur. Although in some cases the disappearance of the electron plasma oscillations from the ionograms may be caused by high temperature, gradual decrease of the signal duration indicates that the rapid increase in the flow velocity of the plasma surrounding the spacecraft is the main reason.

This paper summarizes the results of the measurement of 552 orbits mainly over a period from August 4, 2005 to August 17, 2007. The coverage of data is not homogeneous with respect to solar zenith angle (SZA) and altitude. Also, this data covers a time period with moderate to low solar activity and, does not provide information about the full solar cycle.

2. Detection of the flow velocity boundary

Mars does not possess an active dynamo, as suggested by the Mariner 4 data (Smith et al., 1965; Van Allen et al., 1965) and confirmed later by Mars Global Surveyor (MGS) with closer flybys. Instead, Mars has strong, small scale, remnant crustal magnetic fields (Acuña et al., 1998, 1999; Ness et al., 1999). Due to the lack of a global intrinsic magnetic field, the solar wind interacts directly with the upper atmosphere and ionosphere of Mars (Dubinin et al., 2007). Nevertheless, several plasma boundaries have been identified at Mars. One permanent boundary is the bow shock (BS), which stands between the solar wind and magnetosheath. Bow shocks are produced due to the presence of the planet with a conducting ionosphere which acts as an obstacle in the supersonic solar wind flow (Luhmann and Brace, 1991). The bow shock at Mars was first identified using information gathered during the Mariner-4 fly-by (for observational history see Trotignon et al., 2006). According to Trotignon et al. (2006), the distance of the bow shock from planetary center is around 1.63 R_M at the subsolar point, and 2.63 R_M at the terminator (R_M = 3393 km).

Several types of boundaries have been identified between the shocked solar wind and the ionosphere. Depending on the parameters that can be measured with a given instrument, different methods are used to identify these boundaries. As a consequence, these boundaries have been given different names. Rosenbauer et al. (1989) defines "magnetopause" using the data from TAUS instrument on Phobos 2, as the boundary between the magnetosheath and magnetosphere. Magnetopause crossings from Phobos 2 are also shown in Lundin et al. (1989). Riedler et al. (1989) found a boundary using the direction of the magnetic field and the decrease in the magnetic field turbulence. Breus et al. (1991) defined an "ion composition boundary", which is a boundary between the region dominated by the solar wind protons and plasma of planetary origin. Sauer et al. (1995) reported a "protonopause", at which the heavy ion density becomes comparable to the solar wind proton density. The ion composition boundary and the protonopause are found to be very close to each other (Oieroset et al., 2004). Using a magnetometer and an electron reflectometer (MAG/ER), MGS was able to identify a magnetic pile-up region (Vignes et al., 2000; Oieroset et al., 2004). This boundary was named the magnetic pile-up boundary (MPB) by the MGS team, because of the close similarity to the magnetic field pile-up boundary observed at comets (Acuña et al., 1998; Cloutier et al., 1999; Bertucci et al., 2003; Trotignon et al., 2006). Using ion and electron measurements Lundin et al. (2004) defined what they called an induced magnetospheric boundary. Trotignon et al. (1996) introduced a boundary called "planetopause", which coincides with the ion composition boundary (Oieroset et al., 2004). Closer to Mars, there is a change in the superthermal electron spectrum, which has been defined as photoelectron boundary (PEB) (Nagy et al., 2004). According to Dubinin et al. (2007), there is a clear gap between PEB and MPB, which shows that these two boundaries are, in many cases, separate. It has been suggested that the PEB is associated with the ionopause (Mitchell et al., 2001).

As stated before, the analysis of the boundary between ionosphere and magnetosphere depends on the quantity observed. In this study, we use the duration of the wave packet, which provides us information about the plasma flow velocity at the position of the spacecraft, to obtain the boundary between the ionosphere and the shocked solar wind. Fast flowing solar wind plasma sweeps away the wave packet and prevents electron plasma oscillations from being detected by the receiver. As a consequence, the electron plasma oscillations disappear from the ionograms at high altitudes when the spacecraft is in the solar wind or fast magnetosheath. In some passes, where this boundary is sharp, the disappearance of the electron plasma oscillations is very sudden as the spacecraft is ascending. Ones they disappear, they are not observed again until the end of the pass. The altitude difference corresponding to the time resolution of the disappearance of the electron plasma oscillations (7.54 s), varies between about 5 and 10 km depending on the altitude and the trajectory of the spacecraft. In other passes, the electron plasma oscillations disappear and appear a few times before finally becoming undetectable. We consider mostly those cases where we have a sudden disappearance of the electron plasma oscillations. In all of the cases that we have examined, the electron plasma oscillations are observed until the spacecraft reaches a given altitude, and then they are not observed at all, for the remainder of the pass. A good example is shown in the middle panel of Fig. 3, which shows the electron density profile as a function of universal time (UT). Along the x-axis, the UT, longitude, latitude, altitude and local time coverage of the pass are shown. This is a 36 min pass (orbit 2146), which starts at 15:01:37 UT and ends at 15:37:27 UT. For about the first 4.5 min of the pass, electron plasma oscillations were not observed. During this time, electron density information was not obtained. At around 15:06 UT, electron plasma oscillations have suddenly appeared and provided an electron plasma frequency (about 44 kHz), corresponding to an electron density of 24 cm^{-3}. The electron density values increase as the spacecraft altitude decreases and a maximum value of around 9300 cm^{-3} is reached at 288 km. This altitude is very close to the closest approach to the planet, which is 283 km. Then, the electron density begins to decrease while exhibiting some fluctuations. At around 15:35 UT we observe the last electron plasma oscillations in this pass. After this time, electron plasma oscillations are no longer detected. At 15:06 UT and 15:35 UT, where the sudden appearance and disappearance of the electron plasma oscillations are observed, electron spectral observations suggest the interface location between the ionosphere and shocked solar wind (see bottom panel of Fig. 3). Between these times, the spacecraft is in an approximately inert ionosphere, where the relative velocity between the spacecraft and the plasma is assumed to be due to the speed of the spacecraft, which is smaller than 4.5 km/s. Since the wave packet is in the vicinity of the spacecraft for a time interval long enough to be received, we observe the electron plasma oscillations. Outside these times, the spacecraft is in the shocked solar wind/magnetosheath, where the fast flowing plasma carries the wave packet away before it can be detected.

3. Comparison with ASPERA-3 ELS data

A sharp flow velocity boundary, such as that seen in the middle panel of Fig. 3, was detected in 167 of the (2×552 =) 1104 total cases studied. The boundary points are compared with the data obtained by Analyzer of Space Plasma and Energetic Atoms (ASPERA-3) Electron Spectrometer (ELS). The ASPERA-3 instrument is one of the six experiments on board the Mars Express spacecraft. It was designed to study the plasma and neutral gas environment in near-Mars space and to investigate the interactions between the solar wind and atmosphere of Mars. The ASPERA-3 instrument contains an ion mass analyzer (IMA) and a main unit consisting of a neutral particle imager (NPI) a neutral particle detector (NPD), an electron spectrometer (ELS), and a digital processing unit (DPU) all mounted on top of a scan platform (Barabash et al., 2004). The ELS is an ultra-light, low-power electron sensor, with a field of view of $360° \times 4°$. It measures electrons with energies up to 20 keV/q (Frahm et al., 2006). Also, ELS has a low-energy cut-off of 5 eV and low-energy electron observation is prevented when the spacecraft potential is negative.

The transition from the magnetosheath spectra to spectra showing photoelectrons was investigated to determine where the

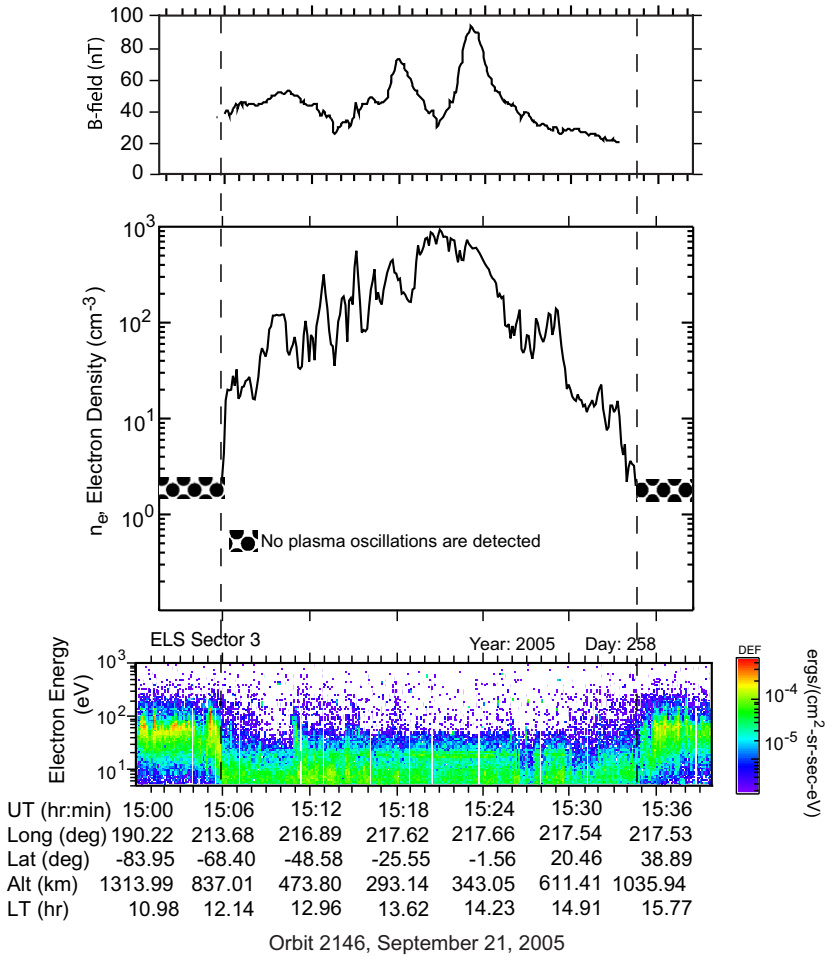

Fig. 3. The magnitude of the local magnetic field from MARSIS (top panel), the local electron density profile from MARSIS (middle panel), and the ASPERA-3 ELS data (bottom panel) are shown for a pass on September 21, 2005. The dashed lines indicate the locations where the electron plasma oscillations disappear.

MARSIS events occur. The bottom panel of Fig. 3 shows the ASPERA-3 ELS data for the orbit 2146. The color code shows the electron energy flux as a function of energy in eV, obtained from ASPERA-3 data. Again, it should be remembered that electrons below 5 eV are not observed by ELS. The electron fluxes above 5 eV are more than two times higher in the magnetosheath than in the ionosphere. Looking at the ASPERA-3 data, we can easily conclude that the ionosphere is between 15:06 UT and 15:35 UT. At these times, there is a big jump in the mean electron energy, where magnetosheath plasma with average energies near about 60 eV is observed. These electron energy enhancement times correspond exactly to the places where, at high altitude, electron plasma oscillations disappear in MARSIS data. The boundaries on both sides of this pass are two of the 158 cases where the boundary is confirmed by the spectral transitions in the ASPERA-3 data. However, the 9 remaining boundary crossings identified by MARSIS data could not be confirmed by the ASPERA-3 data. In 3 of these cases, the electron plasma frequency signature vanishes somewhere inside the magnetosheath. Possibly, the flow speed does not exceed 160 km/s until somewhere in the middle of the magnetosheath and does not coincide with the boundary, giving us a "false boundary point" which is inside the magnetosheath. In the fourth case, electron plasma oscillations disappear about 4 min before the magnetosheath, inside the ionospheric plasma. In the fifth case, the MARSIS boundary point is between the photoelectron boundary and the first occurrence sheath spectra. In the sixth and seventh cases no agreement can be determined because the ELS data is messy. In the eighth case, the electron density drops within a weakened region of ELS electrons and no distinct boundary can be found. Finally, the ninth case has magnetosheath spectra which are determined poorly by ELS, but electron plasma oscillations disappear at the photoelectron boundary. Keeping in mind that the cases where the ASPERA-3 ELS and MARSIS data disagree are only 5% of the total cases, we can conclude that plasma flow velocity boundary on the dayside is a good measure of the boundary between the ionosphere and shocked solar wind.

The top panel of Fig. 3 shows the magnitude of the magnetic field obtained from electron cyclotron echoes using MARSIS data (Gurnett et al., 2005, 2008). In this pass, the electron cyclotron echoes disappear at the same time as the electron plasma oscillations. There is no magnetic field magnitude information at higher altitudes after the boundary. In about 70% of the cases, the magnetic field data ends about the same time as the local electron density data. Therefore, it is not possible to observe changes in the magnetic field occurring at the boundaries. For about 9% of these boundary cases the magnitude of magnetic field data is not available. For the rest of the cases, the magnitude of the magnetic field is obtained on both sides of the boundary. In about one third of these cases, the magnitude of the magnetic field does not show a change. In the remaining, there is a small decrease in the magnitude of the magnetic field going outward, which can mainly be attributed to the influence of crustal magnetic fields.

4. Position of the flow velocity boundary

To obtain the altitude profile of the overall boundary, 158 boundary crossings are sorted according to their SZAs and the boundary altitudes are averaged in 10° SZA bins. As Fig. 4 shows, the average altitude of the flow velocity boundary (black squares) starts at around 750 km near the subsolar point. After a small increase in boundary altitude, the boundary altitude decreases to its lowest value at around 650 km altitude within the SZA range between 20° and 50°. The velocity boundary then begins to increase in altitude as the SZA increases, reaching an average altitude around 1000 km near the terminator. The grey dots in the figure are individual boundary points and vertical lines give the standard deviation at the given SZA range. The data, taken within a two year period from a large range of sampling in both latitude and longitude, are temporal, as well as spatially sampled, which may affect the altitude of the boundary. When individual boundary points at a given SZA range are investigated, large fluctuations in the altitude are observed.

We compared the position of the flow velocity boundary with simulations. Fig. 5 shows a flow speed simulation in the Mars equatorial plane obtained by using a three-dimensional hybrid simulation model which describes the ions fully kinetically and the electrons as a fluid (Modolo et al., 2005). The average flow velocity boundary points obtained from MARSIS data are shown by white squares which are connected by using a white solid line. The plasma speed is given by the color code and contours for 100, 150, 200, 300, and 400 km/s are shown by black solid lines. The dashed line in the figure is the magnetic pile-up boundary as described by Trotignon et al. (2006) and the white solid line starting at around 1.5 R_M is the bow shock obtained from Phobos 2 and MGS data (Trotignon et al., 2006). It should be noted that the MARSIS flow velocity boundary has a similar shape compared to the flow speed contours.

Fig. 6 shows a comparison between the MARSIS flow velocity boundary (squares), the magnetic pile-up boundary as described by Trotignon et al. (2006) (solid line), and the induced magnetospheric boundary as described by Dubinin et al. (2007) (dashed line). The MPB was obtained by using data from Phobos 2 and MGS. The MPB is $1.25 \pm 0.03\ R_M$ at the subsolar point and $1.44 \pm 0.03\ R_M$ at the terminator (Trotignon et al., 2006). The IMB is deduced through the use of ASPERA-3 observations. The IMB is at an altitude which is 0.1 R_M lower than the MPB for SZAs up to around 80°. The altitude of the IMB becomes higher than the MPB for large SZA values. The average boundary from MARSIS coincides mostly with the IMB, with two exceptions. The velocity boundary point at 15° is on top of the MPB and the point at 85° is at a lower altitude than both the MPB and IMB. However, both MPB and IMB are within the error bars of the MARSIS observations.

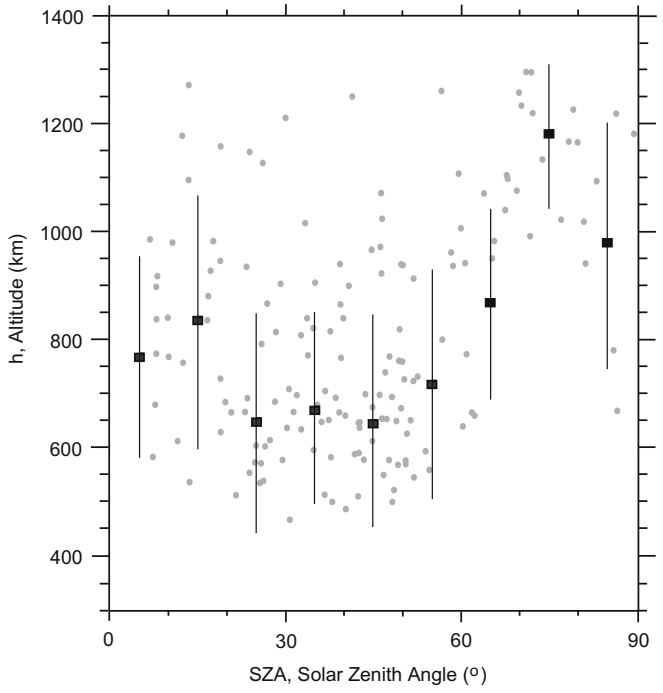

Fig. 4. A plot showing the change in the altitude of the flow velocity boundary as a function of SZA. The black squares in the figure are for the average altitude at a given SZA range. The grey dots show the individual boundary points and the vertical lines give the standard deviation at a given SZA range.

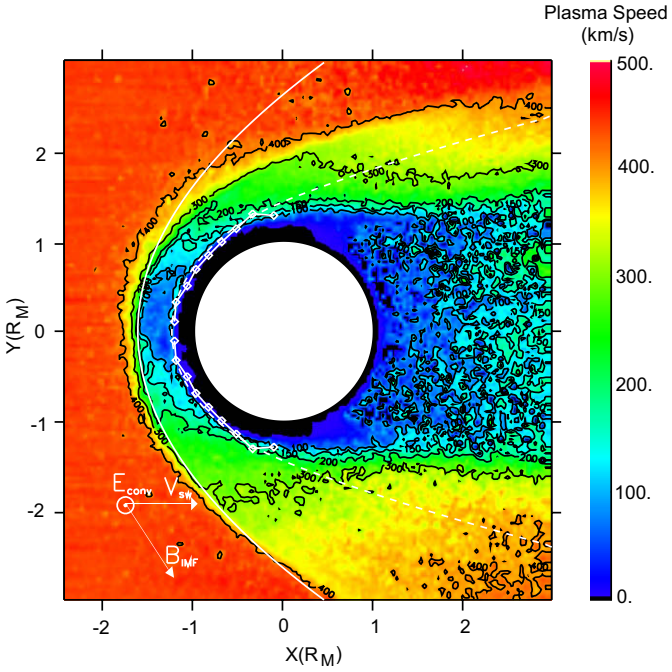

Fig. 5. The average boundary positions obtained from MARSIS are shown on top of the results of plasma flow velocity simulations from a hybrid model. The color code provides the plasma speed in the Mars equatorial plane while the white squares, connected by the white solid line, mark the position of the MARSIS derived flow velocity boundary averaged over 10° of SZA bins. The solid and dashed white lines mark the locations of the bow shock and magnetic pile-up boundary from Trotignon et al. (2006), respectively. Thin, black lines show the contours with the same plasma speed (100, 150, 200, 300 and 400 km).

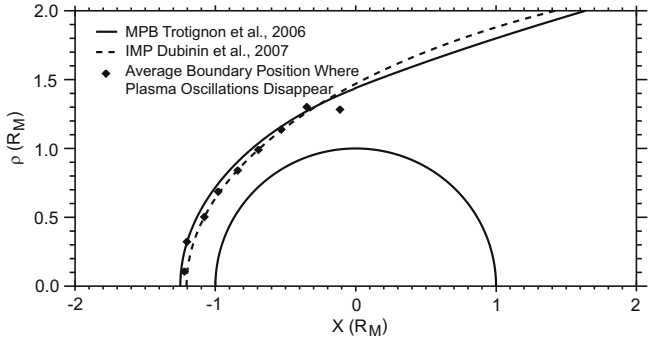

Fig. 6. A comparison of the boundary locations is shown. Here, the boundaries compared are the MPB (solid line) from Trotignon et al. (2006), IMB (dashed line) from Dubinin et al. (2007), and MARSIS flow velocity boundary (squares).

5. Effects of the crustal magnetic fields on the flow velocity boundary

The highly localized crustal magnetic fields can have magnitudes reaching 400 nT in some regions of Mars (Acuña et al., 1998). It is known that these strong crustal magnetic fields can have a considerable effect on the electron density distribution in the ionosphere (Gurnett et al., 2005; Duru et al., 2006). To study possible effects of the crustal magnetic fields on the altitude of the flow velocity boundary, we have computed the magnitude of the magnetic field at 130 km at the latitude and longitude for each boundary point using the Cain et al. (2003) model. This magnetic field model is based on the MGS data. After obtaining the magnitude of the magnetic field at the latitude and longitude of the flow velocity boundary points, the data is divided into two groups: those in the same latitude–longitude location with the magnitude of magnetic field value greater (or less) than 100 nT at 130 km. The average altitude of the boundary location of these two groups, as well as the average of the total data within a given SZA range, are compared in Fig. 7. The green diamonds and red triangles show the altitudes of the boundary averaged over each 10° of SZA for the cases where the magnitude of the crustal magnetic field is less than 100 nT (green diamonds), greater than 100 nT (red triangles). The blue squares give the average altitude. Especially at lower SZA, where we have enough data points to have good statistics, the effect of the strong crustal magnetic fields is observed to increase the altitude of the boundary by approximately 200 km up to a SZA of 60° with respect to cases where the crustal magnetic fields are weak. There is only one SZA range where the average altitude of cases which have the lower crustal magnetic fields is higher than that of the cases which have higher crustal magnetic field magnitudes. Further examining the SZA range between 60° and 70° showed that only one value of the boundary had a magnetic field magnitude higher than 100 nT at 130 km; therefore, this case is not reliable due to low statistics.

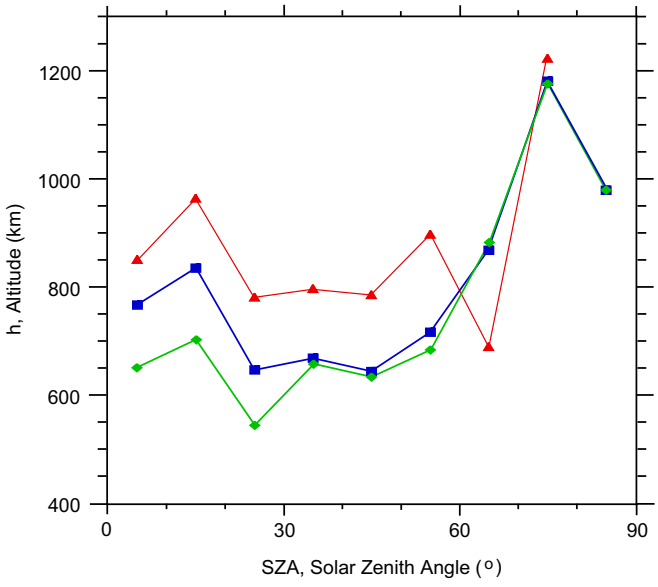

Fig. 7. The average boundary altitudes as a function of SZA are shown for three different groups of data. These groups are (1) an average of all the data (blue squares), (2) a subset of the data which is at the same latitude and longitude location where the crustal magnetic field magnitude is higher than 100 nT at an altitude of 130 km (red triangles), (3) a subset of the data which is at the same longitude and latitude location where the crustal magnetic field magnitude is lower than 100 nT at an altitude of 130 km (green diamonds).

The fact that strong crustal magnetic fields tend to raise the altitude of the magnetic pile-up boundary is confirmed by Crider et al. (2002), studying southern and northern hemispheres, and by Brain et al. (2005), by investigating magnetized and unmagnetized regions. These results are consistent with their findings. Also, Franz et al. (2006) have shown that around the terminator, the MPB altitude is almost a linear function of the strength of the crustal magnetic fields.

In Fig. 8 a pass from November 27, 2007 is displayed as an example of the increase in the altitude of the flow velocity due to strong crustal magnetic fields. The trajectory of this pass is shown in Fig. 9. The pass starts at 09:05:11 UT, at an altitude of 1355 km, and a SZA of 87.06°. The spacecraft is at its lowest altitude, 309 km, between 09:24:41 UT and 09:25:34 UT. At the end of the pass (09:45:03 UT) the spacecraft's altitude is 1343 km and its SZA is 90.11°. In this 40 min pass, two boundary points, at 09:13:06 UT and 09:43:17 UT have been identified, one at each end of the pass. These times, also correspond to the places where there is a big increase in the average electron energy. It is clear from ASPERA-3 ELS data that the locations where the electron plasma oscillations disappear correspond to the boundary between the ionosphere and shocked solar wind. At these two boundary points, which are only 30 min away from each other in time, the SZA values are approximately the same value around the terminator: 86.31° and 89.81°. Therefore, both temporal and SZA effects are ruled out. The crustal magnetic fields from Cain et al. (2003) are shown in the bottom panel. Here, the black line gives the magnitude of the magnetic field. The red, blue and green lines are for the radial, southward and eastward components of the magnetic field, respectively. The crustal magnetic field values at 130 km are computed at the latitude and longitude of these two locations. The magnetic field value for the first point is 9.702 nT at 130 km, and the boundary is at an altitude of 741 km. The magnetic field is found to be 669.4 nT for the second location and the altitude is 1195 km. In a case like this, where it is known that the only substantial difference is in the strength of the crustal magnetic fields, the altitude elevation of the boundary can be directly correlated to the crustal magnetic field strength. It should be stated that, there can be other factors affecting the boundary, such as the interplanetary magnetic field (IMF) clock angle. Unfortunately, we do not have IMF clock angle information. Therefore, we cannot study its effect on the boundary. However, the big increase in the altitude of the boundary where the crustal magnetic fields are strong suggests that crustal magnetic fields have a significant effect on the altitude of the boundary.

6. Conclusion

Using the fact that the electron plasma oscillations at the position of the spacecraft suddenly disappear, a plasma flow velocity boundary on the dayside between the ionosphere and shocked solar wind is determined. In a two year period, 552 orbits are studied and an average position for the flow velocity boundary is obtained. This boundary altitude starts at around 750 km near the subsolar point and after a small drop, constantly increases on the dayside with increasing SZA, eventually reaching about 1000 km around the terminator. When the individual boundary crossings are studied, it is seen that the altitude of individual points is highly fluctuating. In fact, the standard deviation of the points in a given 10° solar zenith angle range is around 200 km in many SZA ranges.

We compared this boundary with the plasma flow velocity simulations computed using a hybrid model. The shape of contours which have similar speeds agrees with the shape of MARSIS boundary.

We analyzed whether the plasma flow velocity boundary coincides with the photoelectron boundary or the MPB as defined by

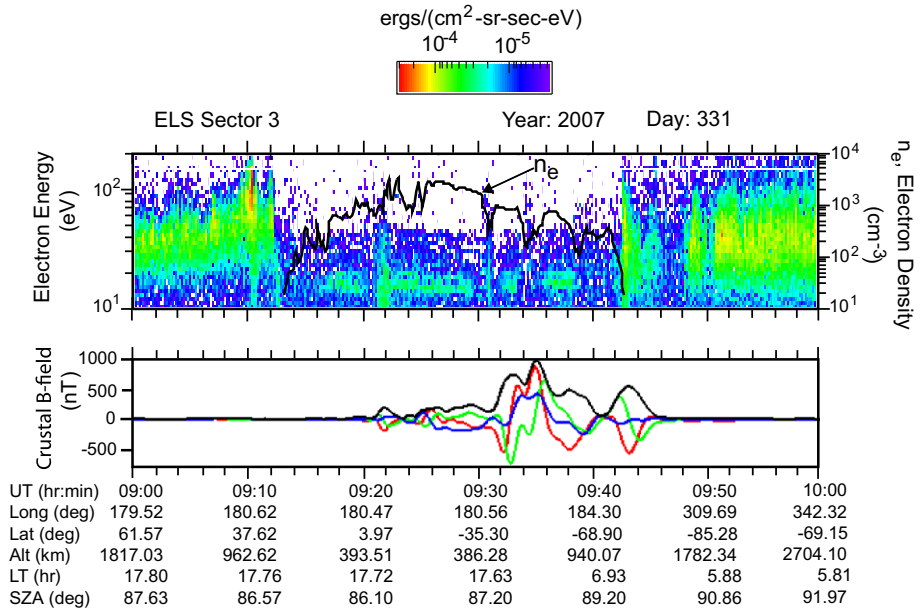

Fig. 8. The local electron density data from MARSIS and electron spectra from ASPERA-3 ELS are shown together for the pass on November 27, 2007. The bottom panel gives the crustal magnetic fields from Cain et al. (2003). In this panel, the magnitude of the magnetic field is given by the black line. The radial, southward and eastward components of the magnetic field are given by the red, blue and green lines, respectively. Two flow velocity boundary locations on each side of the pass have been identified. The one at the location with strong crustal magnetic fields is at about 450 km higher altitude than the other boundary.

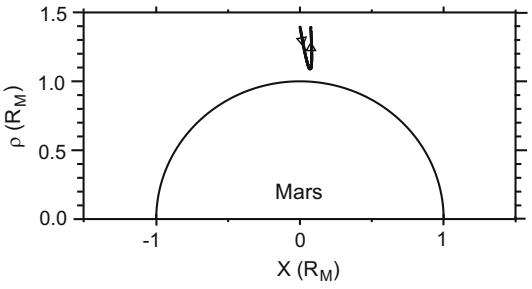

Fig. 9. Shown is the trajectory of the Mars Express spacecraft on November 27, 2007 for the data shown in Fig. 8, in which the X direction is along the Mars–Sun line and $\rho = (y^2 + z^2)^{1/2}$. This plot is drawn in cylindrical coordinates.

the 60 eV flux. Whenever there is a clear separation between these two boundaries, MARSIS flow velocity boundary agrees with the 60 eV flux boundary, except a few cases where the electron plasma oscillations end before the beginning of the sheath plasma. The plasma flow velocity boundary is observed at larger distance than the photoelectron boundary and coincides with the start of the magnetosheath plasma. Unfortunately, for the period studied in this paper we do not have information on planetary ions. Therefore, we cannot determine any possible changes of ion species when the plasma flow velocity boundary is crossed.

The comparison of the flow velocity boundary with the magnetic pile-up boundary determined using Phobos 2 and MGS data, and the induced magnetospheric boundary determined using ASPERA-3 data show that the plasma oscillation boundary is in good agreement with these other boundaries. There are some SZA ranges where there is $\sim 0.1\ R_M$ difference between the altitude of the MARSIS flow velocity boundary and the altitudes of IMB and MPB. However, when the standard deviation in a given SZA range is studied, it is seen that both of the boundaries are within the error bars of the MARSIS boundary.

Finally, analysis of a correlation between the crustal magnetic fields and the position of the plasma flow velocity boundary reveals that the altitude of the boundary is higher at locations where the crustal magnetic fields are strong. This effect can be seen more clearly at lower SZA where a good amount of data is present. In the lower SZA region (SZA < ~30°), the average altitude of the data set with strong crustal magnetic fields is about 200 km (or more) higher than the altitude of the data set with weak crustal magnetic fields.

Acknowledgments

Research at the University of Iowa was funded by contract 1224107 with the Jet Propulsion Laboratory.

References

Acuña, M.H.and 19 colleagues, 1998. Magnetic field and plasma observations at Mars: Initial results of the Mars global surveyor mission. Science 279, 1676–1680.

Acuña, M.H.and 12 colleagues, 1999. Global distribution of crustal magnetization discovered by the Mars global surveyor MAG/ER experiment. Science 284, 790–793.

Barabash, S., and 45 colleagues. 2004. ASPERA-3: Analyzer of Space Plasmas and Energetic Ions for Mars Express, Mars Express: The scientific payload. In: Andrew Wilson (Ed.), Scientific Coordination: Agustin Chicarro. ESA SP-1240, Noordwijk, The Netherlands: ESA Publications Division, ISBN 92-9092-556-6, pp. 121–139.

Bertucci, C.and 11 colleagues, 2003. Magnetic field draping enhancement at the martian magnetic pileup boundary from Mars global surveyor observations. Geophys. Res. Lett. 30, 1099. 71-1–71-4.

Brain, D.A., Halekas, J.S., Lillis, R., Mitchell, D.L., Lin, R.P., 2005. Variability of the altitude of the martian sheath. Geophys. Res. Lett. 32, L18203.

Breus, T.K., Krymskii, A.M., Lundin, R., Dubinin, E.M., Luhmann, J.G., Yeroshenko, Ye.G., Barabash, S.V., Mitnitskii, V.Ya., Pissarenko, N.F., Styashkin, V.A., 1991. The solar wind interaction with Mars: Consideration of Phobos 2 mission observations of an ion composition boundary on the dayside. J. Geophys. Res. 96, 11165–11174.

Cain, J.C., Ferguson, B.B., Mozzoni, D., 2003. An $n = 90$ internal potential function of the martian crustal magnetic field. J. Geophys. Res. 108 (E2), 5008. doi:10.1029/2000JE001487.

Chicarro, A., Martin, P., Traunter, R., 2004. Mars Express: A European mission to the red planet. In: Wilson, A. (Ed.), MARS EXPRESS, The Scientific Payload, SP-1240. ESA Publication Division, Noordwijk, Netherlands, pp. 3–16.

Cloutier, P.A.and 19 colleagues, 1999. Venus-like interaction of the solar wind with Mars. Geophys. Res. Lett. 26, 2685–2688.

Crider, D.H.and 12 colleagues, 2002. Observations of the latitude dependence of the location of the martian magnetic pileup boundary. Geophys. Res. Lett. 29, 1170. 11-1–11-4.

Dubinin, E., Franz, M., Woch, J., Roussos, E., Barabash, S., Lundin, R., Winningham, J.D., Frahm, R.A., Acuña, M., 2007. Plasma morphology at Mars. ASPERA-3 observations. Space Sci. Rev. 126, 209–238.

Duru, F., Gurnett, D.A., Averkamp, T.F., Kirchner, D.L., Huff, R.L., Persoon, A.M., Plaut, J.J., Picardi, G., 2006. Magnetically controlled structures in the ionosphere of Mars. J. Geophys. Res. 111, A11204. doi:10.1029/2006JA011975.

Duru, F., Gurnett, D.A., Morgan, D.D., Modolo, R., Nagy, A., Najib, D., 2008. Electron densities in the upper ionosphere of Mars from the excitation of electron plasma oscillations. J. Geophys. Res. 113, A07302. doi:10.1029/2008JA013073.

Frahm, R.A.and 15 colleagues, 2006. Location of atmospheric photoelectron energy peaks within the Mars environment. Space Sci. Rev. 126, 389–402.

Franz, M.and 44 colleagues, 2006. Plasma intrusion above Mars crustal fields—Mars Express ASPERA-3 observations. ICARUS 182, 406–412.

Gurnett, D.A., Bhattacharjee, A., 2005. Introduction to Plasma Physics with Space and Laboratory Applications. Cambridge University Press, Cambridge.

Gurnett, D.A.and 10 colleagues, 2005. Radar soundings of the ionosphere of Mars. Science 310, 1929–1933.

Gurnett, D.A., and 10 colleagues. 2008. An overview of radar soundings of the martian ionosphere from the Mars Express spacecraft. J. Adv. Space Res. doi:10.1016/j.asr.2007.01.062.

Luhmann, J.G., Brace, L.H., 1991. Near-Mars space. Rev. Geophys. 29, 121–140.

Lundin, R., Zakharov, A., Pellinen, R., Borg, H., Hultqvist, B., Pissarenko, N., Dubinin, E.M., Barabash, S.W., Liede, I., Koskinen, H., 1989. First measurements of the ionospheric plasma escape from Mars. Nature 341, 609–612.

Lundin, R.and 44 colleagues, 2004. Solar wind-induced atmospheric erosion at Mars: First results from ASPERA-3 on Mars express. Science 305, 1933–1936. doi:10.1126/science.1101860.

Mitchell, D.L., Lin, R.P., Mazelle, C., Réme, H., Cloutier, P.A., Connerney, J.E.P., Acuña, M.H., Ness, N.F., 2001. Probing Mars' crustal magnetic field and the ionosphere with the MGS electron reflectometer. J. Geophys. Res. 106. 23,419–23427.

Modolo, R., Chanteur, G.M., Dubinin, E., Matthews, A.P., 2005. Influence of the solar EUV flux on the martian plasma environment. Ann. Geophysicae 23, 433–444.

Nagy, A.F.and 14 colleagues, 2004. The plasma environment of Mars. Space Sci. Rev. 111, 33–114.

Ness, N.F., Acuña, M.H., Connerney, J., Wasilewski, P., Mazelle, C., Sauvaud, J., Vignes, D., d'Uston, C., Reme, H., Lin, R., Mitchell, D.L., McFadden, J., Curtis, D., Cloutier, P., Bauer, S.J., 1999. MGS magnetic fields and electron reflectometer investigation: Discovery of paleomagnetic fields due to crustal remnance. Adv. Space Res. 23 (11), 1879–1886.

Oieroset, M., Mitchell, D.L., Phan, T.D., Lin, R.P., Crider, D.H., Acuña, M.H., 2004. The magnetic field pile-up and density depletion in the martian magnetosheath: A comparison with the plasma depletion layer upstream of the Earth's magnetopause. Space Sci. Rev. 111, 185–202.

Picardi, G.and 12 colleagues, 2004. Mars Express: A European Mission to the Red Planet, SP-1240. ESA Publication Division, Noordwijk, Netherlands. pp. 51–70.

Riedler, W.and 32 colleagues, 1989. Magnetic fields near Mars: First results. Nature 341, 604–607.

Rosenbauer, H.and 20 colleagues, 1989. Ions of martian origin and plasma sheet in the martian magnetosphere: Initial results of the TAUS experiment. Nature 341, 612.

Sauer, K., Bogdanov, A., Baumgartel, K., 1995. The protonopause—An ion composition boundary in the magnetosheath of comets. Venus and Mars. Adv. Space Res. 16 (4)153–(4)158.

Smith, E.J., Davis Jr., L., Coleman Jr., P.J., Jones, D.E., 1965. Magnetic field measurements near Mars. Science 149, 1241–1242.

Trotignon, J.G., Dubinin, E., Grard, R., Barabash, S., Lundin, R., 1996. Martian planetopause as seen by the plasma wave system onboard Phobos 2. J. Geophys. Res. 101, A11, 24965–24977.

Trotignon, J.G., Mazelle, C., Bertucci, C., Acuña, M.H., 2006. Martian shock and magnetic pile-up boundary positions and shapes determined from the Phobos 2 and Mars Global Surveyor data sets. Planet. Space Sci. 54, 357–369.

Van Allen, J.A., Frank, L.A., Krimigis, S.M., Hillis, H.K., 1965. Absence of martian radiation belts and implications thereof. Science 149, 1228–1233.

Vignes, D., Mazelle, C., Reme, H., Acuña, M.H., Connerney, J.E.P., Lin, R.P., Mitchell, D.L., Cloutier, P., Crider, D.H., Ness, N.F., 2000. The solar wind interaction with Mars: Locations and shapes of the bow shock and the magnetic pile-up boundary from the observations of the MAG/ER experiment onboard Mars Global Surveyor. Geophys. Res. Lett. 27, 49–52.